Journal of Power Sources 196 (2011) 5478–5484

Contents lists available at ScienceDirect

Journal of Power Sources

journal homepage: www.elsevier.com/locate/jpowsour

Fe-based perovskites as electrodes for intermediate-temperature solid oxide fuel cells

Shu-en Hou [a], Ainara Aguadero [b,*], José Antonio Alonso [b], John B. Goodenough [c]

[a] Engineering Research Center of Nano-Geo Materials of Ministry of Education, China University of Geosciences, Wuhan 430074, China
[b] Instituto de Ciencia de Materiales de Madrid, CSIC, Cantoblanco, E-28049 Madrid, Spain
[c] Texas Materials Institute, ETC 9.102, The University of Texas at Austin, Austin, TX 78712, USA

ARTICLE INFO

Article history:
Received 14 October 2010
Received in revised form
12 November 2010
Accepted 20 November 2010
Available online 26 November 2010

Keywords:
Intermediate-temperature SOFC
MIEC oxide
$SrFeO_3$
Double perovskite
Hydrogen

ABSTRACT

A solid-oxide fuel cell (SOFC) based upon Fe perovskites, has been designed and tested. Materials with nominal compositions $Sr_{0.9}K_{0.1}FeO_{3-\delta}$ (SKFO) and $Sr_{1.6}K_{0.4}FeMoO_{6-\delta}$ (SKFMO) with perovskite structure have been prepared and characterized as cathode and anode, respectively. The anode material exhibits high electrical conductivity values of 407–452 S cm^{-1} at 750–820 °C in pure H_2. In the test cells, the electrodes were supported on a 300-μm-thick pellet of the electrolyte $La_{0.8}Sr_{0.2}Ga_{0.83}Mg_{0.17}O_{3-\delta}$ (LSGM). The single SOFC cells gave a maximum power density at 850 °C of 937 mW cm^{-2} with pure H_2 as a fuel. Sizeable power densities were also observed with alternative fuels: 694 and 499 mW cm^{-2} with H_2 containing 5 parts per million of H_2S and CH_4, respectively, at 800 °C. Moreover, only a slight degradation of about 3.6% of the power density has been obtained after 65 different cycles of fuel-cell test in H_2 at 750 °C and 14% at 850 °C in 50 cycles using H_2–H_2S. This remarkable behavior has been correlated to the structural features determined in a neutron powder diffraction experiment in the usual working conditions of a SOFC for a cathode (air) and an anode (low pO_2). On the one hand, the cubic *Pm-3m* $Sr_{0.9}K_{0.1}FeO_{3-\delta}$ cathode material is an oxygen deficient perovskite with oxygen contents that vary from 2.45(2) to 2.26(2) from 600 to 900 °C and high oxygen isotropic thermal factors (4.17(8) Å^2) suggesting a high ionic mobility. On the other hand, the actual nature of the anode of composition $Sr_{1.6}K_{0.4}FeMoO_{6-\delta}$ has been unveiled by neutron powder diffraction to consist of two main perovskite phases with the compositions $SrMoO_3$ and $SrFe_{0.6}Mo_{0.4}O_{2.7}$. The association of two perovskites oxides, $SrMoO_3$ with high electrical conductivity, and $SrFe_{0.6}Mo_{0.4}O_{2.7}$ with mixed ionic–electronic conductivity has resulted in an extraordinarily performing anode material for SOFCs.

1. Introduction

Solid oxide fuel cells (SOFCs) exhibit higher efficiency and are less sensitive to fuel impurities than fuel cells working at low temperatures, so the former can operate under a wide variety of fuels (e.g. hydrogen, methane, carbon monoxide, naphtha, gas oil, kerosene, gases of biomass and landfill wastes). However, reduction of the operating temperature to the 500–850 °C range while keeping a high performance is one of the major requirements for viable commercialization of these devices. To this end, the development of mixed ionic–electronic conductors (MIECs) as electrodes with an adequate performance at the lower temperatures is one of the challenges [1]. Therefore, extensive attempts to identify catalytically active MIECs suitable for both the anode and the cathode continue to be made.

Regarding the cathode, stabilization of a 3C perovskite framework based upon the $SrCoO_{3-\delta}$ system has been a widely used strategy to obtain an adequate mixed ionic–electronic conductor in air at the operating temperature. For this purpose, several chemical substitutions have been performed at either the Sr (partially replaced by Ba, La, Sm) [2] or Co (partly replaced by Sc, Fe, Ni, Sb, etc.) [3,4] positions, or at both. The most extensively used derivatives of $SrCoO_{3-\delta}$ are $Ba_{0.5}Sr_{0.5}Co_{0.8}Fe_{0.2}O_{3-\delta}$ (BSCF) [5], $SrCo_{0.8}Fe_{0.2}O_{3-\delta}$ (SCF) [6,7] and $La_{1-x}Sr_xFe_{1-y}Co_yO_{3-\delta}$ [8–10] due to their high oxygen fluxes and favorable oxygen-reduction performance at temperatures ≥600 °C. However, these materials show moderate electronic conductivities (~35 S cm^{-1}) [11], which could be one of the problems responsible for their low performance at temperatures below 600 °C [5,12]. The $SrCo_{0.95}Sb_{0.05}O_{3-\delta}$ perovskite has been shown to be an excellent cathode with high

* Corresponding author. Tel.: +34 91 3349000; fax: +34 913720623.
E-mail addresses: ainara.aguadero@icmm.csic.es, ainara.aguadero@gmail.com (A. Aguadero).

0378-7753/$ – see front matter © 2010 Elsevier B.V. All rights reserved.
doi:10.1016/j.jpowsour.2010.11.122

electronic conductivity (500 S cm^{-1} at 400 °C) and very low polarization resistances [13,14]. Nevertheless, Co is too expensive even when partially substituted by other metals and it is associated with a too high thermal expansion related to the other cell components. In a previous work, we have developed a Co-free $Sr_{0.9}K_{0.1}FeO_{3-\delta}$ perovskite with very appealing properties as a SOFC cathode; the introduction of K in the $SrFeO_{3-\delta}$ perovskite has a twofold effect [15]: on the one hand, the larger ionic radius of K^+ (1.64 Å) with respect to Sr^{2+} (1.44 Å) combined with the hole-doping effect induces an increase of the tolerance factor, favoring the stabilization of an untilted crystal structure with Fe–O–Fe angles of 180°, which maximizes the Fe–O–Fe interactions. On the other hand, the presence the K would boost the Fe valence, which favors the introduction of oxygen vacancies at high temperature, to promote an adequate ionic conductivity at the working temperature. A single-cell test based upon $Sr_{0.9}K_{0.1}FeO_{3-\delta}$ as cathode, Sr_2MgMoO_6 as anode, and $La_{0.8}Sr_{0.2}Ga_{0.83}Mg_{0.17}O_{3-\delta}$ (LSGM) as electrolyte gave maximum power densities of 680 mW cm^{-2} at 800 °C and 850 mW cm^{-2} at 850 °C with pure H_2 as fuel [15].

Concerning the anode, the conventional Ni-YSZ cermets catalyze carbon formation during direct oxidation of hydrocarbon fuels and suffer from sintering problems during the cell operation [16–18]. Moreover, Ni-based anodes are susceptible to sulphur poisoning [19], whereas copper–ceria cermets (Cu–CeO_2) lack adequate catalytic activity and thermal stability. The development of MIEC oxides stable under reducing atmosphere is one important topic under investigation. Several works have demonstrated a great performance of Mo-based double perovskites operating in H_2 or CH_4 as a fuel [20]. The development of a Co-free anode based upon the Sr_2FeMoO_6 system with adequate mixed ionic–electronic conductivity, sulphur tolerance, and operating either in H_2 or CH_4 as a fuel was our goal. For this purpose, single cells have been set up and tested using $Sr_{1.6}K_{0.4}FeMoO_6$ (SKFMO) as anode, $Sr_{0.9}K_{0.1}FeO_{3-\delta}$ (SKFO) as cathode and LSGM as electrolyte. The present NPD study of the thermal evolution of the crystal structure of both electrodes helped to unveil several key features to understand their performance in a single cell.

2. Experimental

The syntheses of the $Sr_{0.9}K_{0.1}FeO_{3-\delta}$ (SKFO) and $Sr_{1.6}K_{0.4}FeMoO_{6-\delta}$ (SKFMO) materials were performed with a standard ceramic procedure. For SKFO, stoichiometric amounts of analytical grade $Sr(CH_3COO)_2$, $K_2C_2O_4{\cdot}H_2O$ and $Fe(CH_3COO)_2$ were heated in air in alumina crucibles at 900 °C for 15 h, 1000 °C for 15 h, and 1100 °C for 10 h with intermediate grindings, followed by ball milling for 40 min. For SKFMO, stoichiometric amounts of $Sr(CH_3COO)_2$, $K_2C_2O_4{\cdot}H_2O$, $Fe(NO_3)_9{\cdot}H_2O$ and $(NH_4)_6Mo_7O_{24}{\cdot}4H_2O$ were ground and calcined at 800 °C for 10 h and 1200 °C for 20 h and, after ball milling the powder, reduced at 850 °C for 12 h in pure H_2.

In order to assess phase purity, X-ray diffraction (XRD) analysis was performed with a Philips X-pert diffractometer (40 kV, 30 mA) in Bragg–Brentano reflection geometry with Cu Kα radiation (λ = 1.5418 Å). For the characterization of the electrodes, neutron powder diffraction (NPD) is a powerful tool [21] to examine, *in situ*, the electrodes under the usual conditions of a SOFC (air for the cathode, and low pO_2 atmosphere for the anode). Neutron powder diffraction (NPD) patterns were collected at the Institut Laue-Langevin, Grenoble (France) as a function of temperature at the D2B diffractometer with λ = 1.594 Å. The SKFO cathode material was contained in a quartz tube open to the air and placed in a vanadium furnace. The NPD patterns were collected at RT, 600, 800 and 930 °C. On the other hand, SKFMO was placed in a vanadium can introduced into a vanadium furnace and the experiment was carried out under vacuum. The NPD patterns were collected at 250, 500, 750, 850 and 930 °C. NPD diffraction patterns were analysed by the Rietveld method [22] with the FULLPROF refinement program [23]. A pseudo-Voigt function was chosen to generate the line shape of the diffraction peaks. The coherent scattering lengths for K, Sr, Fe, Mo and O were: 3.67, 7.020, 9.75, 6.715 and 5.803 fm, respectively. The following parameters were refined in the final run: scale factor, background coefficients, zero-point error, pseudo-Voigt corrected for asymmetry parameters, positional coordinates, and isotropic displacement factors.

The electrical conductivity of dense bars was measured for the reduced SKFMO sample from 200 to 850 °C in pure H_2, 5% H_2–95% Ar, CH_4, and air by the *dc* four-probe method. A current load of 10–100 mA was applied and the potential drop was recorded in an RG&G Princeton Applied Research 273 Potentiostat-Galvanostat.

Single-cell tests were carried out on electrolyte-supported cells using $La_{0.8}Sr_{0.2}Ga_{0.83}Mg_{0.17}O_{3-\delta}$ (LSGM) as electrolyte. The LSGM pellets of 20-mm diameter were sintered at 1450 °C for 20 h and then polished with a diamond wheel to a thickness of 300 μm. $La_{0.4}Ce_{0.6}O_{2-\delta}$ (LDC) was used as a buffer layer between the anode and the electrolyte in order to prevent the interdiffusion of ionic species between perovskite and electrolyte. Inks of LDC, SKFO and SKFMO were prepared with a binder (V-006 from Heraeus). LDC ink was screen-printed onto one side of the LSGM disk followed by a thermal treatment at 1300 °C in air for 1 h. SKFMO was subsequently screen printed onto the LDC layer and fired at 1275 °C in air. SKFO was finally screen printed onto the other side of the disk and fired at 1100 °C for 1 h. The working electrode area of the cell was 0.24 cm^2 (0.6 cm × 0.4 cm). Reference electrodes of the same materials as the working electrodes were used to monitor the overpotentials of the cathode and anode in the cell configuration [24,25]. The reference electrodes were deposited 5 mm apart from the working electrodes and with an area of 0.04 cm^2 (0.2 cm × 0.2 cm). Pt gauze with a small amount of Pt paste in separate dots was used as current collector at both the anodic and the cathodic sides for ensuring electrical contact. The cells were tested in a vertical tubular furnace at 750, 800, and 850 °C; the anode side was fed with different fuels of pure H_2, H_2–H_2S, and CH_4 with a flow of 20 ml min^{-1}, whereas the cathode worked in an air flow of 100 ml min^{-1}.

The fuel-cell tests were performed with an EG&G potentiostat/galvanostat by changing the voltage of the cell from 1.28 to 0.2 V, with steps of 0.030 V, holding 10 s at each step. Current density was calculated by the recorded current flux through the effective area of the cell (0.24 cm^2). The electrolyte voltage drop was calculated from the electrolyte conductivity obtained by *ac* impedance spectroscopy in air in previous experiments [24,25]. The stability of the cell was evaluated by performing the fuel-cell test from 1.28 V to 0.2 V and back to 1.28 V in several cycles.

Scanning electron microscopy was used to study the cross-sectional layers of the SKFO/LSGM/LDC/SKMFO cells in a JEOLJSM-5610 instrument.

3. Results and discussion

3.1. In situ NPD determination of the crystal structures

SKFO was prepared as a polycrystalline powder; its crystal structure at room temperature (RT) was defined from XRD data as tetragonal *P4/mmm* with minor amounts of $Sr_3Fe_2O_{6.75}$ as a secondary phase [15]. The SKFMO oxide was successfully obtained as a black, well crystallized powder. As shown in Fig. 1a, XRD data showed no evidence of impurities or starting materials in the prepared powders and all the reflections were apparently characteristic of a cubic perovskite for both the SKFO and the SKFMO

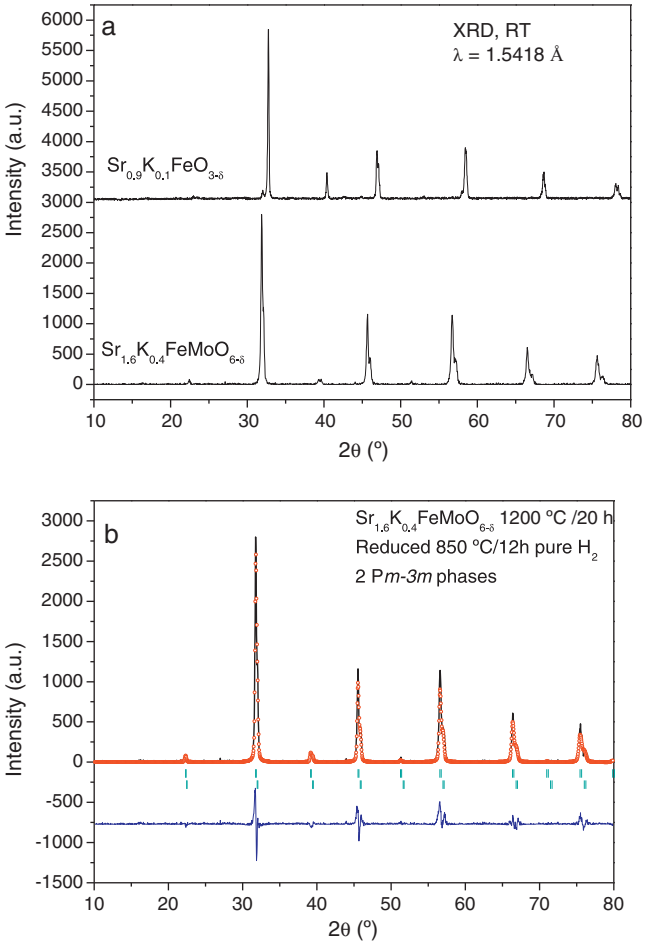

Fig. 1. (a) X-ray diffraction diagrams of $Sr_{0.9}K_{0.1}FeO_{3-\delta}$ and $Sr_{1.6}K_{0.4}FeMoO_{6-\delta}$. (b) Rietveld plot of $Sr_{1.6}K_{0.4}FeMoO_{6-\delta}$ refined with a two-perovskite phase model.

phases. However, a more exhaustive Rietveld analysis of the crystal structure of SKFMO at RT reveals a very poor fitting between the experimental and the calculated XRD profiles due to the appearance of extra features or shoulders in the experimental profile. Attempts to refine the structure in less symmetric space groups did not improve the fitting. Finally, the introduction of two cubic *Pm-3m* phases with slightly different unit-cell parameters ($a = 3.98135(4)$ and $a = 3.9561(9)$ Å) allowed us to satisfactorily improve the profile fitting. Fig. 1b illustrates the final Rietveld plot obtained, where all the shoulders are accounted for by the second perovskite phase. More details on the nature of both perovskite oxides were determined from the neutron experiments.

The thermal evolution of the crystal structure of the SKFO cathode material was studied by NPD; the data were collected *in situ* in a quartz tube open to the air in the usual working temperature range of a SOFC, 600–930 °C. At 600 °C the crystal structure of the sample was Rietveld-refined in the cubic *Pm-3m* space group. In spite of the irregular background due to the quartz container, a good agreement between observed and calculated profiles was achieved (Fig. 2). Subsequent structural refinement of NPD data collected at 800 and 930 °C was also successfully refined in this *Pm-3m* space group. Table 1 summarizes the main structural features determined for this cathode material.

The thermal evolution of the oxygen content in air was also studied by neutron powder diffraction. Fig. 3 shows the temperature dependence of the concentration of oxygen vacancies (δ) and unit-cell parameters for SKFO. The oxygen content decreases when heating the sample in air from a virtually stoichiomet-

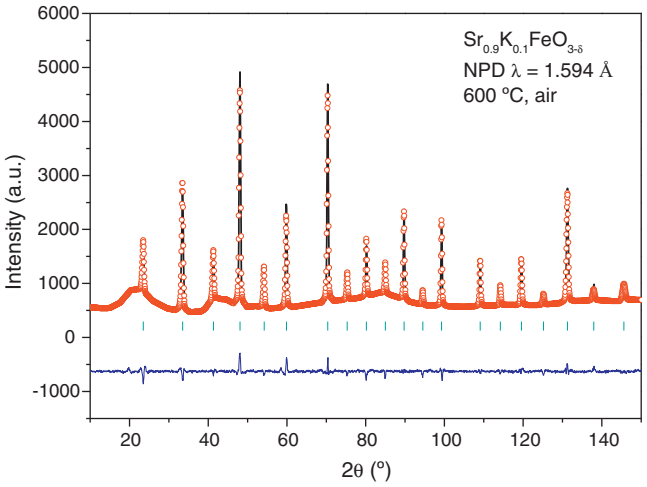

Fig. 2. Observed (open circles), calculated (full line) and difference (at the bottom) NPD profiles for $Sr_{0.9}K_{0.1}FeO_{3-\delta}$ at 600 °C in air refined in the cubic *Pm-3m*. The vertical markers correspond to the allowed Bragg reflections. The irregular background is due to the quartz container.

Table 1
Unit-cell, thermal parameters and main bond distances (Å) for $K_{0.1}Sr_{0.9}FeO_{3-\delta}$ refined in the cubic *Pm-3m* space group from NPD data at 600 °C, 800 °C and 930 °C in air. Reliability factors are also included.

	600 °C	800 °C	930 °C
a (Å)	3.91298(7)	3.9397(1)	3.9597(2)
V (Å)^3	59.913(2)	61.149(3)	62.084(4)
	(*Sr*, *K*) 1b (1/2 1/2 1/2)		
B (Å)^2	1.92(4)	2.49(5)	3.16(6)
	(*Fe*) 1a (0 0 0)		
B (Å)^2	1.81(4)	2.52(4)	3.21(5)
	O_1 3d (1/2 0 0)		
Focc	0.82	0.77	0.75
B (Å)^2	2.72(5)	3.42(7)	4.17(8)
Reliability factors			
χ^2	6.85	6.31	5.32
R_p%	2.90	2.82	2.51
R_{wp}%	3.90	3.83	3.47
R_{bragg}%	3.25	3.64	2.83
AO_{12} polyhedra A = Sr, K			
A–O_1	2.76688(4)	2.78576(6)	2.79992(8)
FeO_6 octahedra			
Fe–O_1	1.95648(4)	1.96983(6)	1.97981(8)

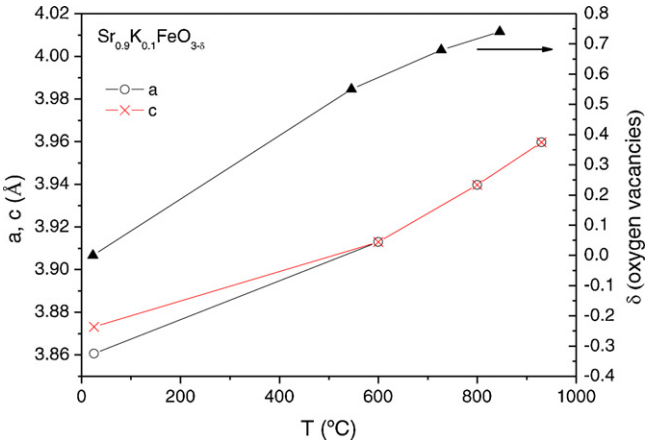

Fig. 3. Thermal variation of unit-cell parameters and oxygen vacancies (δ) contents of $Sr_{0.9}K_{0.1}FeO_{3-\delta}$ from *in situ* NPD data. A phase transition from tetragonal to cubic occurs between RT and 600 °C.

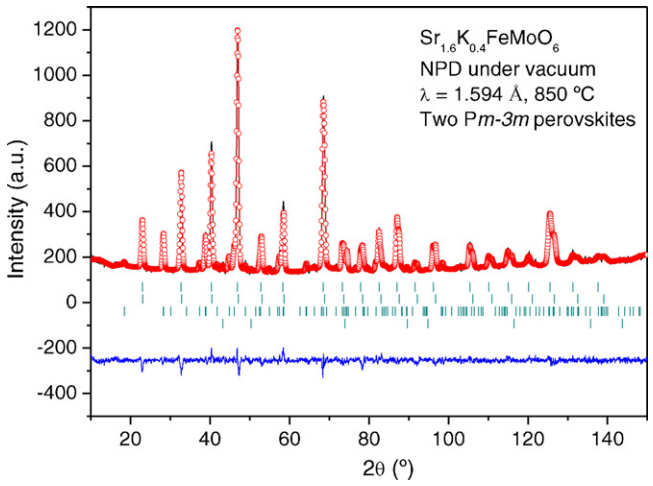

Fig. 4. Rietveld refinement of the $Sr_{1.6}K_{0.4}FeMoO_{6-\delta}$ structure at 850 °C using a two-*Pm-3m* phases model. The two last series of Bragg-reflection markers correspond to minor $SrMoO_4$ and Fe impurity phases.

ric $Sr_{0.9}K_{0.1}FeO_{2.96(4)}$ at RT to a highly reduced $Sr_{0.9}K_{0.1}FeO_{2.26(2)}$ at 930 °C. The oxygen contents at 600 and 800 °C were 2.45(2) and 2.32(2), respectively. The isotropic displacement factors (B) of the oxygen atoms increase from 2.72(5) Å^2 (600 °C) to 4.17(8) Å^2 (930 °C) indicating a high mobility or chemical lability of these oxygens, thus suggesting a high ionic conductivity at the working temperatures of the SOFC. It is important to note that there is a change of the slope in the thermal evolution of the a unit-cell parameter at 600 °C. Above this temperature the expansion is higher; this might be due to the association of two effects at elevated temperatures; on the one hand the expected thermal expansion due to the increase in the lattice vibrations and, on the other hand, the expansion due to the progressive reduction of the Fe oxidation state from 4+ at RT to 3+ at 600 °C, 2.74+ at 800 °C and 2.62+ at 930 °C.

Secondly, the thermal evolution of the crystal structure of the SKFMO material used as anode was also evaluated by NPD. For this purpose, the sample was contained in a vanadium can under high vacuum (10^{-6} torr) and the NPD data were collected at 250, 500, 750, 850, and 930 °C. An initial attempt to refine the crystal structure in the cubic *Pm-3m* space group showed the existence of some extra reflections corresponding to the $SrMoO_4$ scheelite and Fe metal as secondary phases. Furthermore, the analysis of the diffraction data with the simple cubic perovskite and the two secondary phases reveals a very poor fitting between the experimental and the calculated NPD profiles due to the appearance of extra features or shoulders in the experimental profile, as commented above for the treatment of the XRD data; attempts to refine the structure in less symmetric space groups did not improve the quality of the fitting. The introduction of two cubic phases with slightly different unit-cell parameters and with a strong degree of overlapping of the low-angle reflections led to a satisfactorily agreement between observed and calculated profiles. Fig. 4 illustrates the final refinement at 850 °C, successfully performed with a four-phase model consisting of two cubic perovskite phases and the two $SrMoO_4$ scheelite and Fe metal minor impurity phases. Table 2 lists the structural parameters obtained for both cubic phases at 750 °C. From the refinement of the occupancy factors of both perovskite structures, the following compositions have been determined for all the temperatures: $SrMoO_3$ and $SrFe_{0.6}Mo_{0.4}O_{3-\delta}$. The $SrMoO_3$ cubic perovskite is oxygen stoichiometric (according to the refinement of the occupancy factors for the oxygen atoms) and has been reported to present one of the highest electrical conductivity values at room temperature for a ceramic material (~10^4 S cm^{-1}) [26].

Table 2
Unit-cell, thermal parameters and main bond distances (Å) for two main crystallographic phases required to describe $K_{0.4}Sr_{1.6}FeMoO_{6-\delta}$ in the cubic *Pm-3m* space group from NPD data at 750 °C. Reliability factors are also included.

	$SrMoO_3$	$SrFe_{0.6}Mo_{0.4}O_{3-\delta}$
a (Å)	4.0048(1)	3.9830(2)
V (Å)^3	64.229(4)	63.187(4)
	(*Sr*) 1b (1/2 1/2 1/2)	
B (Å)^2	2.55(8)	2.7(1)
	(*Mo*) 1a (0 0 0)	(*Fe*, *Mo*) 1a (0 0 0)
B (Å)^2	0.98(7)	2.36(7)
	O_1 3d (1/2 0 0)	
Focc	1.0	0.93
B (Å)^2	2.53(5)	3.28(9)
Fract (%)[a]	49.9	32.3
R_{bragg}%	4.55	6.9
AO_{12} polyhedra A = Sr		
A–O_1	2.83182(5)	2.8164(5)
Fe,MoO_6 octahedra		
B–O_1	2.00240(5)	1.9915(1)
Reliability factors		
χ^2	2.75	
R_p%	3.21	
R_{wp}%	4.08	

[a] The remain is 17% $SrMoO_4$ and 0.5% Fe.

Moreover, the accompanying $SrFe_{0.6}Mo_{0.4}O_{3-\delta}$ oxygen-defective perovskite, containing about 0.3 oxygen vacancies per formula unit, seems to contribute sufficiently high oxide-ion conductivity in the usual working conditions of an anode in a SOFC. Fig. 5 displays the thermal evolution of the lattice parameters and isotropic thermal factors of the oxygen atoms for both perovskite phases; no structural transitions have been observed in the measured temperature range.

3.2. Electrical conductivity

Fig. 6 shows the thermal variation of the electrical conductivity of SKFMO measured in different atmospheres. In air the conductivity increases with temperature up to 0.6 S cm^{-1} at 600 °C. As the atmosphere becomes more reducing, from 5% H_2–Ar to pure H_2, the material becomes metallic and the electrical conductivity increases reaching in the temperature range of 750–820 °C the values of 14.7–19.0 and 407–452 S cm^{-1}, respectively, for the two atmospheres. Under CH_4, the SKFMO oxide shows a semiconductor-like behavior in all the temperature range studied, displaying a maximum conductivity of 11.8 S cm^{-1} at 820 °C.

3.3. Fuel-cell test

The performance of $Sr_{1.6}K_{0.4}FeMoO_{6-\delta}$ as anode and $Sr_{0.9}K_{0.1}FeO_{3-\delta}$ as cathode was tested in single cells in an electrolyte-supported configuration using a 300-μm-thick LSGM electrolyte. Fig. 7 shows the cell voltage and power density as a function of current density at 750, 800 and 850 °C for the single cells fed with pure H_2, H_2 containing 5 parts per million of H_2S and CH_4 as fuels. In H_2 the maximum power densities generated by the cell are 586, 766 and 937 mW cm^{-2} for temperatures of 750, 800 and 850 °C, respectively. In H_2–H_2S the maximum power densities yield 598, 695 and 797 mW cm^{-2} at 750, 800, and 850 °C, respectively. The use of CH_4 as fuel leads to a considerable decrease of the cell performance; in this case the maximum power densities drop to values of 109, 189 and 399 mW cm^{-2} at 750, 800, and 850 °C, respectively.

The anode and cathode overpotentials (η_a and η_c) as a function of the current density for H_2, H_2–H_2S and CH_4 at 750, 800, and 850 °C are shown in Fig. 8. The dependences of η_a and η_c on the current density agree well with that of the power density. For all

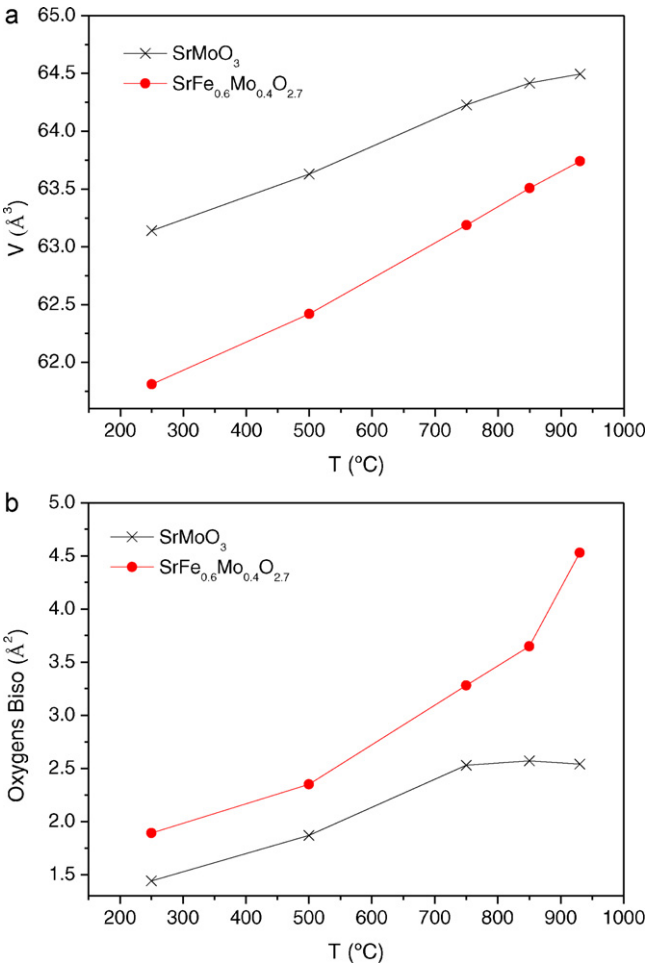

Fig. 5. Thermal variation of (a) unit cell *a* parameters and (b) isotropic thermal factors for oxygen atoms for the two perovskite phases $SrMoO_3$ and $SrFe_{0.6}Mo_{0.4}O_{2.7}$.

the cases under study, the cathode overpotential is higher than that of the anode as previously observed for other systems [20].

Fig. 9 shows a SEM micrograph of the cross section of the cathodic and anodic sides of the cell carried out after the single-cell tests. A good adherence between electrolyte and electrodes is observed, without cracking problems after the temperature cycling under H_2. The thickness of SKFO is about 50 μm whereas a layer of 20 μm thick of SKFMO is deposited over a 30 μm thick LDC. It is also apparent that the electrolyte presents high density and the electrodes exhibit an adequate porosity.

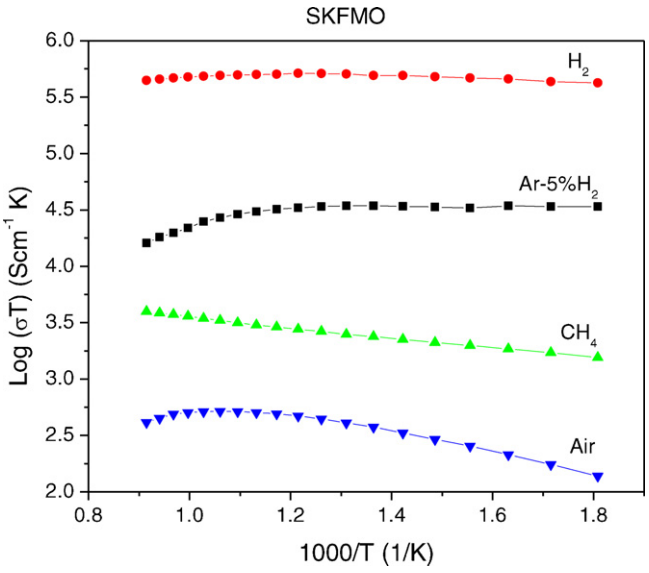

Fig. 6. Electrical conductivity $Sr_{1.6}K_{0.4}FeMoO_{6-\delta}$ under different atmospheres.

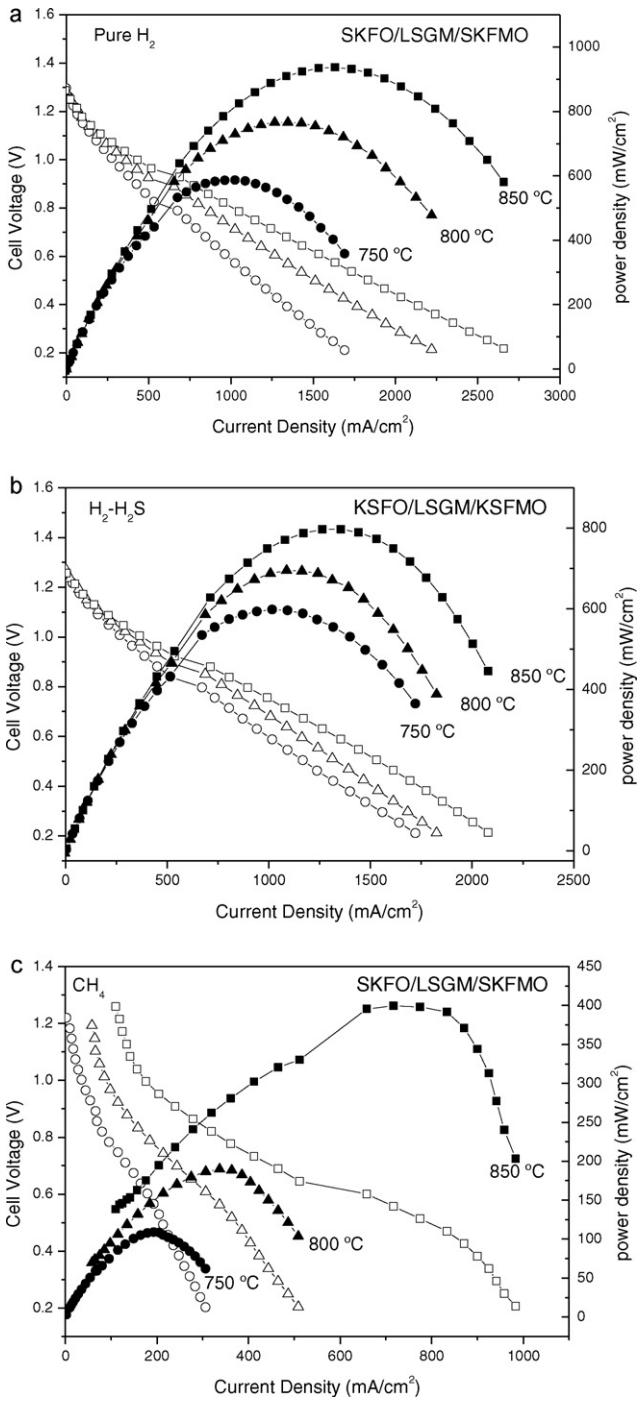

Fig. 7. Cell voltage (left axis) and power density (right axis) as a function of the current density for the test cell with the configuration SKFMO/LDC/LSGM/SKFO (a) in pure H_2, (b) in H_2–H_2S and (c) in CH_4.

In order to test the stability of the cell, we ran the cells for repeated power cycles of 20 min from 1.28 V to 0.2 V and back to 1.28 V. Fig. 10a shows the maximum power density at 750 °C obtained in 65 different number of power cycles of fuel-cell test in H_2. A slight degradation of about 3.6% of the power density

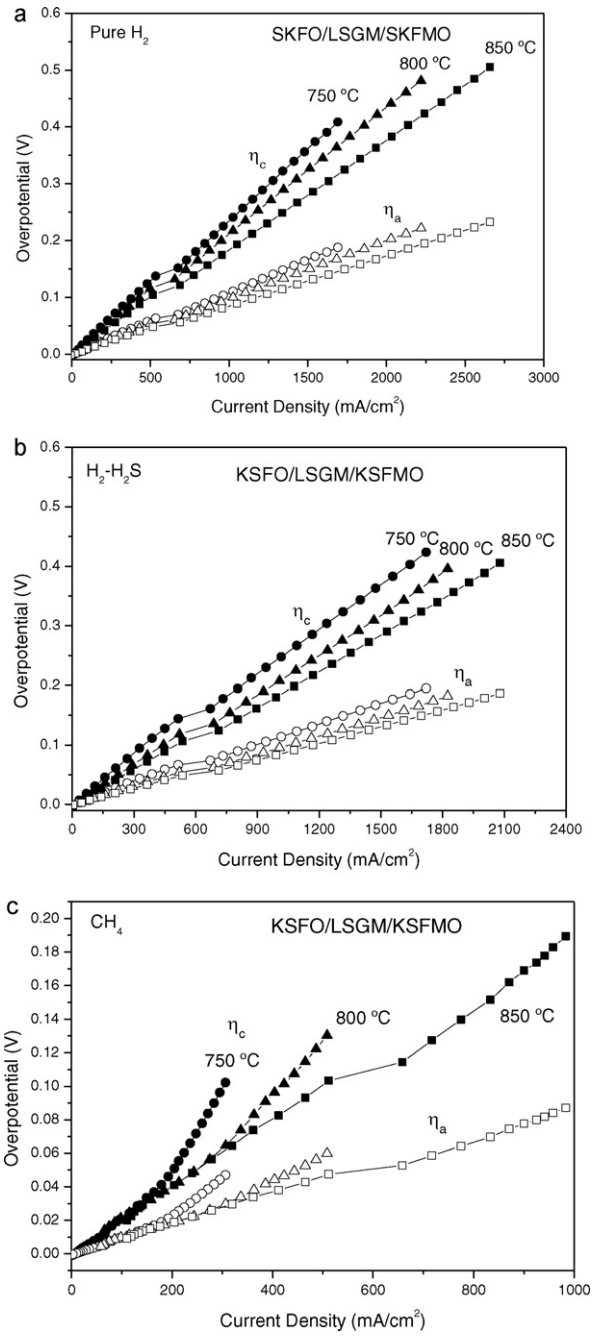

Fig. 8. Anodic and cathodic overpotentials for test cells with $Sr_{1.6}K_{0.4}FeMoO_{6-\delta}$ and $Sr_{0.9}K_{0.1}FeO_{3-\delta}$ as anodic and cathodic materials (a) in pure H_2, (b) in H_2–H_2S and (c) in CH_4.

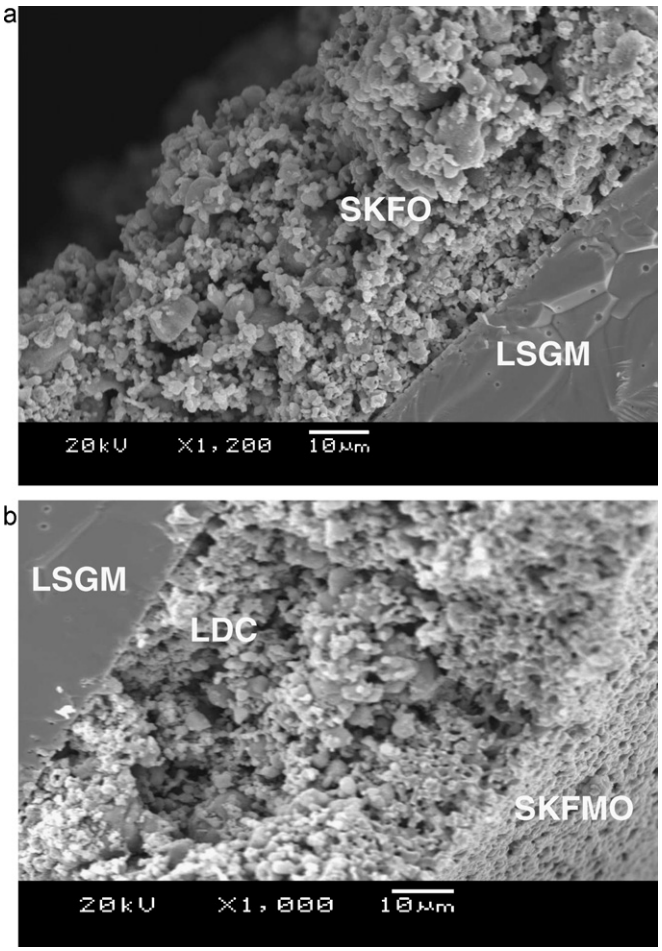

Fig. 9. Cross-section SEM images of (a) the SKFO/LSGM cathode side and (b) the anode side SKFMO/LDC/LSGM after the fuel cell test under H_2.

is observed at the end of the experiment. However, the stability test performed at 850 °C in H_2–H_2S gave a more important performance degradation of 14% after 50 cycles and 20% after 100 cycles (Fig. 10b), probably due to the sulphur poisoning of the anode.

The described test-cell shows an excellent performance of the SKFO/LSGM/SKFMO SOFC configuration with a maximum power density of 937 mW cm^{-2} and a non-negligible power of 766 mW cm^{-2} at 800 °C with pure H_2 as a fuel, amply surpassing the requirements of 500 mW cm^{-2} at 800 °C for practical use of a single cell. It also exhibits a good cyclability with little power loss up to 65 cycles. The anode material shows a good fuel flexibility, yielding almost 400 mW cm^{-2} with CH_4 as a fuel. Moreover, both cathode and anode overpotentials take small values, below 0.1 V at a current density of 500 mA cm^{-2} at 800 °C, and therefore the cathodic/anodic losses are no longer rate-determining for the output power of the cell. The ohmic loss across the electrolyte is now rate limiting since the concentration overpotentials are not likely to be rate limiting at those current densities with H_2 fuel and thick film electrodes. Therefore, a foreseeable way to improve the performance would be to make either anode- or cathode-supported cells, thus reducing the thickness of the electrolyte to a minimum value.

We can correlate the good performance observed in the single-cell test with the structural features obtained from the "*in situ*" neutron powder diffraction experiment in the usual working conditions of a cathode (air) and an anode (low pO_2) in a SOFC. On the one hand, we have observed that the cathode $Sr_{0.9}K_{0.1}FeO_{3-\delta}$ is a cubic *Pm-3m* perovskite with an oxygen content that varies from 2.45(2) to 2.26(2) oxygens per formula unit from 600 to 900 °C. Remarkably, it is among the most oxygen deficient perovskites ever reported, comparable to $Sr_{0.2}Ba_{0.8}CoO_{2.27(1)}$ [27]. Furthermore, the isotropic thermal factors (B) of the oxygen atoms increase from 2.72(5) to 4.17(8) Å^2 in the same temperature range, indicating a high mobility or chemical lability of these oxygen atoms and suggesting a high ionic conductivity.

On the other hand, the neutron experiment allowed us to unravel the actual nature of the anodic material. In fact it is a composite consisting of two main cubic perovskite phases, $SrMoO_3$ and $SrFe_{0.6}Mo_{0.4}O_{2.7}$, the former characterized by an elevated electronic conductivity whereas the latter combines a mixed ionic–electronic conduction mechanism. In fact, double perovskites

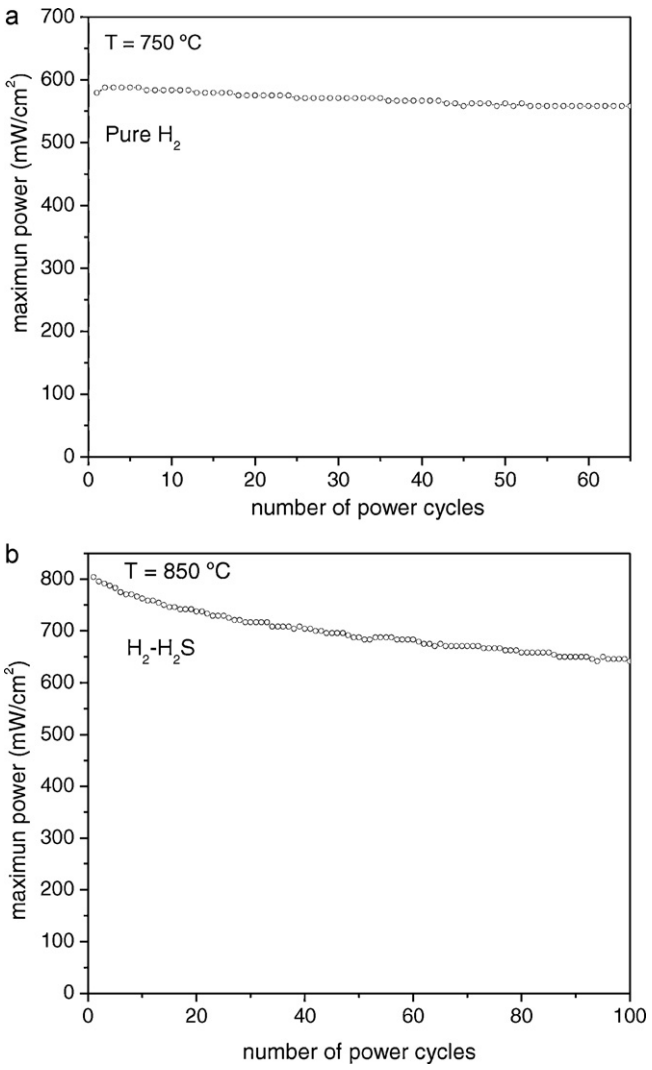

Fig. 10. Stability of the cell performance versus the number of power cycles in (a) pure H_2 and (b) H_2–H_2S. The cells for repeated power cycles of 20 min from 1.28 V to 0.2 V and back to 1.28 V.

of the type $Sr_2BB'O_6$, containing two transition metal ions at the B positions, have been demonstrated to be an excellent alternative to the standard cermets (Ni+YSZ) and to exhibit an excellent performance in single cells in hydrogen and methane [20,28]. The double perovskite Sr_2FeMoO_6 (written as $SrFe_{0.5}Mo_{0.5}O_3$ in the absence of long-range Fe/Mo ordering) is well-known for its magneto resistance properties, based upon its simultaneous ferromagnetic and half-metallic behavior [29,30]. The absence of potassium in the refined stoichiometry of the present $SrFe_{0.6}Mo_{0.4}O_{2.7}$ perovskite is probably related to the high synthesis temperature, involving the sublimation of this element. However, the presence of potassium in the starting composition seems to be essential to produce an anode material with adequate texture and final composition, giving rise to the observed segregation into two main perovskite components. Trials to utilize directly the standard Sr_2FeMoO_6 double perovskite as anode led to an extremely low performance. In the present case, the association of these two main perovskite components results in an anode material with an extraordinary performance in single-cell tests, with a good stability along several operating cycles with H_2 as fuel and non-negligible fuel flexibility in the 750–850 °C temperature range.

4. Conclusions

SKFO and SKFMO have been successfully utilized as cathode and anode materials, respectively, in single SOFC cells with LSGM as electrolyte. A maximum power density of 937 mW cm^{-2} was obtained at 850 °C with pure H_2 as fuel, whereas non-negligible power outputs were reached with alternative fuels such a CH_4. We can correlate the good performance observed in the single-cell tests with the structural features obtained from NPD data collected in the usual working conditions of a cathode (air) and an anode (low pO_2) in a SOFC. The cathode is a cubic perovskite $Sr_{0.9}K_{0.1}FeO_{3-\delta}$ between 600 °C and 800 °C displaying an oxygen content that varies from 2.45(2) to 2.26(2), respectively. The oxygen atoms exhibit high isotropic thermal factors suggesting a high ionic conductivity. The extraordinary performance of the anode material relies on the association of the two main cubic perovskite phases, combining a high electronic and ionic conductivity under reducing conditions and an adequate fuel flexibility.

Acknowledgements

We are grateful to ILL for making the beamtime available. JBG thanks the NSF and Robert A. Welch Foundation of Houston, TX, for financial support (Grant #F-1066). JAA acknowledges the financial support of the Spanish "Ministerio de Ciencia e Innovación" (MICINN) to the project MAT2010-16404 and during his sabbatical. A.A. also thanks to MICINN for a "Juan de la Cierva" contract.

References

[1] S.B. Adler, Chem. Rev. 104 (2004) 4791–4843.
[2] T. Nagai, W. Ito, T.R. Sakon, Solid State Ionics 177 (2007) 3433–3444.
[3] Z. Deng, Q.W. Liu, C.S. Chen, H. Lu, W.S. Yang, Solid State Ionics 170 (2004) 187–190.
[4] P. Zeng, R. Ranj, Z. Chen, W. Zhou, H. Gu, Z. Shao, S. Liu, J. Alloys Compd. 455 (2008) 465–470.
[5] Z.P. Shao, H.S. Maile, Nature 431 (2004) 170.
[6] W. Zhou, R. Ran, Z. Shao, J. Power Sources, 195 (2010) 3386–3393.
[7] J.J. Tunney, M.L. Post, X. Du, D. Yang, J. Electrochem. Soc. 149 (2002) H113.
[8] J. Chen, F. Liang, B. Chi, J. Pu, S.P. Jiang, L. Jian, J. Power Sources 194 (2009) 275.
[9] J. Chen, F. Liang, D. Yan, J. Pu, B. Chi, S.P. Jiang, L. Jian, J. Power Sources 195 (2010) 5201.
[10] J. Chen, F. Liang, L. Liu, S. Jiang, B. Chi, J. Pu, J. Li, J. Power Sources 183 (2008) 586.
[11] B. Wei, Z. Lü, X. Huang, J. Miao, X. Sha, X. Xin, W. Su, J. Eur. Ceram. Soc. 26 (2006) 2827.
[12] J. Peña-Martínez, D. Marrero-Lopez, J.C. Ruiz-Morales, B.E. Buergler, P. Nuñez, L. Gauckler, J. Solid State Ionics 177 (2006) 2143.
[13] A. Aguadero, D. Pérez-Coll, C. De la Calle, J.A. Alonso, M.J. Escudero, L. Daza, J. Power Sources 192 (2009) 132–137.
[14] A. Aguadero, J.A. Alonso, C. de la Calle, M.T. Fernández-Díaz, Chem. Mater. 12 (2010) 789–798.
[15] S. Hou, J.A. Alonso, J.B. Goodenough, J. Power Sources 195 (2010) 280–284.
[16] S.P. Jiang, S.H. Chan, Mater Sci. Technol. 20 (2004) 1109.
[17] B.C.H. Steele, I. Kelly, M. Middleton, R. Rudkin, Solid State Ionics 28–30 (1988) 1547.
[18] Y. Matsuzaki, I. Yasuta, Solid State Ionics 132 (2000) 261.
[19] J.H. Wang, M. Liu, Electrochem. Commun. 9 (2007) 2212.
[20] Y.H. Huang, R.I. Dass, Z.-L. Xing, J.B. Goodenough, Science 312 (2006) 254–257.
[21] J.A. Alonso, M.J. Martínez-Lope, A. Aguadero, L. Daza, Prog. Solid State Chem. 36 (2008) 134–150.
[22] H.M. Rietveld, J. Appl. Crystallogr. 2 (1969) 65.
[23] J. Rodríguez-Carvajal, Physica B 192 (1993) 55.
[24] J.-H. Wan, J.-Q. Yan, J.B. Goodenough, J. Electrochem. Soc. 152 (2005) A1511.
[25] M. Feng, J.B. Goodenough, K. Huang, C. Milliken, J. Power Sources 63 (1996) 47.
[26] B.L. Chamberland, P.S. Danielson, J. Solid State Chem. 3 (1971) 243–247.
[27] C. de la Calle, J.A. Alonso, A. Aguadero, M.T. Fernández-Díaz, F. Porcher, Z. Kristallogr., 225 (2010) 209–215.
[28] J.B. Goodenough, Y.H. Huang, J. Power Sources 173 (2007) 1.
[29] K.I. Kobayashi, T. Kimura, H. Sawada, K. Terakura, Y. Tokura, Nature 395 (1998) 677.
[30] M. Retuerto, J.A. Alonso, M.J. Martinez-Lope, J.L. Martinez, M. García-Hernández, Appl. Phys. Lett. 85 (2004) 266.